Strombolian eruptions and dynamics of magma degassing at Yasur Volcano (Vanuatu)

Julia Woitischek[1,2], Andrew W. Woods[1,2], Marie Edmonds[1], Clive Oppenheimer[3], Alessandro Aiuppa[4], Tom D. Pering[5], Tehnuka Ilanko[5], Roberto D'Aleo[6], Esline Garaebiti[7]

[1] Department of Earth Sciences, University of Cambridge, Downing Street, Cambridge, CB2 3 EQ, United Kingdom

[2] BP Institute, University of Cambridge, Madingley Road, Cambridge, CB3 OEZ, United Kingdom

[3] Department of Geography, University of Cambridge, Downing Pl, Cambridge, CB2 3EN, United Kingdom

[4] Dipartimento di Scienze della Terra e del Mare (DiSTEM), Universita degli Studi di Palermo, Via Archirafi 36, Palermo 90123, Italy

[5] Department of Geography, University of Sheffield, Winter Street, Sheffield, S10 2TN, United Kingdom

[6] INGV, Sezione di Palermo, Via Ugo la Malfa 153, 90146, Palermo, Italy

[7] Vanuatu Meteorology and Geohazards Department, Lini Highway, Port Vila, Vanuatu

Highlights:

- FTIR and Multi-GAS measurements at Yasur Volcano constrain volcanic gas compositions
- A new model is proposed to explain the cyclic variation in gas geochemistry at Yasur, based on rupture and reforming of a crystal-rich plug.
- High fluxes of volcanic gases have persisted at Yasur Volcano for decades.

Abstract

Open vent basaltic volcanoes account for a substantial portion of the global atmospheric outgassing flux, largely through passive degassing and mild explosive activity. We present volcanic gas flux and composition data from Yasur Volcano, Vanuatu collected in July 2018. The average volcanic plume chemistry is characterised by a mean molar CO_2/SO_2 ratio of 2.14, H_2O/SO_2 of 148 and SO_2/HCl of 1.02. The measured mean SO_2 flux in the period of 6th to 9th July is 4.9 kg s^{-1}. Therefore, the mean fluxes of the other species are 7.5 kg·s^{-1} CO_2, 208 kg·s^{-1} H_2O and 4.8 kg·s^{-1} HCl. The degassing regime at Yasur volcano ranges from 'passive' to 'active' styles, with the latter including Strombolian activity and spattering. Gases emitted during active degassing are enriched in SO_2 over HCl and CO_2 over SO_2 relative to passive degassing, with CO_2/SO_2 ratios of 2.85 ± 0.17, SO_2/HCl of 1.6 ±0.22, and H_2O/SO_2 of 315 ± 78.8. Gases emitted during passive degassing have CO_2/SO_2 ratios of 1.96 ± 0.12, SO_2/HCl of

0.50 ±0.07 and H_2O/SO_2 of 174 ± 43.5. We use a model of volatile degassing derived from melt inclusion studies (Metrich et al., 2011), combined with our observations of chemical variations in the outgassing bubbles to propose a mechanism for magma degassing in the conduit at Yasur. We envisage a shallow conduit filled with crystal-rich magma, forming a viscous and mobile plug that develops an effective yield strength from the surface to a depth of at least 2000 m, in which bubbles are trapped, grow, ascend towards the surface and burst in a typical Strombolian eruption. Deeper bubbles released during active degassing are enriched in CO_2 and SO_2 compared to bubbles released during 'passive degassing', which are sourced from close to the surface, and are, consequently, HCl-rich.

Keywords: basaltic open vent volcanoes, Strombolian activity, Yasur, crystal content in magma, gas fluxes, magma fluxes.

1. Introduction

Basaltic volcanoes contribute a large proportion of the volcanic gas flux to the atmosphere (Burton et al., 2013, Aiuppa et al., 2019). Six of the ten most prolific volcanic outgassers are basaltic open-vent volcanoes (Burton et al., 2013, Carn et al., 2017), wherein degassing takes place from the free magma surface at an open vent. Characterising this style of degassing is important in order to monitor volcanic hazard, understand their role in the geochemical cycling of volatiles between the interior and atmosphere on a planetary scale, and quantify the volumes and depths of the magma bodies responsible for driving the degassing. The activity observed at basaltic open-vent volcanoes is characterised by a range of degassing regimes, from passive degassing and lava lake activity, through Strombolian activity, lava fountaining and sub-Plinian eruptions (e.g. Blackburn et al, 1976, Williams, 1983, Walker et al., 1984, Coltelli et al.,1995, Allard et al., 2005, Burton et al., 2007a, Aiuppa et al., 2010, Ilyinskaya et al., 2012, Tamburello et al., 2012). These styles of activity are dependent, to varying degrees, on magma rise speed, magma volatile content, bubble-melt separation depth, bubble ascent velocity and bulk magma viscosity (Wilson and Head, 1981, 1983, Parfitt and Wilson, 1995, Slezin, 2003, Houghton and Gonnerman, 2008).

Strombolian activity is associated with the bursting of large bubbles termed gas slugs (or Taylor bubbles) at the vent or lava lake surface (Blackburn et al., 1976, Sparks, 1978, Burton et al., 2007a, Houghton and Gonnermann, 2008, Parfitt, E.A., 2004, Pering et al., 2015). It is common at basaltic volcanoes because the comparatively low viscosity of the melt (10 - 10^4 Pa·s) allows

gas-melt segregation and bubble coalescence processes on the timescale of magma rise (Batchelor, 1967, Jaupart and Vergniolle, 1988, 1989, Woods and Cardoso, 1997, Francis and Oppenheimer, 2004, Parfitt and Wilson, 2008, James et al., 2009,). Gas slugs can range in length up to 200 m (Taddeucci et al., 2010, Del Bello et al., 2012,). The rise of a large gas bubble or slug is often accompanied by an increase in the height of the magma surface until the bubble bursts at the surface and releases a large volume of magmatic gas, ejecting metre-scale molten magma fragments and ash into the air (Taddeucci et al., 2012a,b, Gaudin et al., 2016, Houghton et al., 2008). Typical volumes of gas released by a single bubble at Stromboli vary from 10 – 1000 m^3 (Vergniolle and Brandeis, 1996, Ripepe and Marchetti, 2002, Mori and Burton, 2009, Del Bello et al., 2012, Pering and McGonigle, 2018). Another key characteristic of Strombolian eruptions is periodic or quasi-periodic, short-duration eruptions (5-6 events of 5-10 seconds duration per hour) (Allard et al., 1994, Ripepe and Harris., 2008, Taddeucci et al., 2012a,b, Houghton et al., 2016, Gaudin et al., 2016).

Among the volcanoes that exhibited Strombolian behaviour are Stromboli (Italy), Pacaya (Guatemala), Erebus (Antarctica), Villarrica (Chile), Reventador (Ecuador), Arenal (Costa Rica) and Yasur (Vanuatu) (Ntepe and Dorel, 1990, Neuberg et al., 1994, Vergniolle and Brandeis, 1996, Seyfriend and Hort, 1999, Chouet et al., 1999,2003, Urbanski et al., 2002, Hort et al., 2003, Oppenheimer et al., 2006, Ripepe et al., 2007; Patrick et al., 2007, Gaudin et al., 2014, Ripepe et al., 1993). Strombolian activity is characterised by discrete, rhythmic, mild to moderate bursting of over-pressurised bubbles lasting for a few seconds, with a low eruption rate of a variety of pyroclastics including lapilli, bombs, ash and lithic blocks (Rosi et al., 2013, Houghton et al., 2016). This typical activity can be subdivided qualitatively into normal, major and paroxysmal kinds of explosion (Rosi et al., 2013) or, based on the products of the explosion, into ballistic- or ash-dominated explosions (Rosi et al., 2013, Patrick et al., 2007, Gaudin et al., 2017). The transition between these different types of eruption is still not well understood but might correlate with the slug size and the presence of a layer of degassed and cooled magma on top (Del Bello et al., 2015, Capponi et al., 2016, Spina et al., 2019b, Oppenheimer et al., 2020)

Between Strombolian eruptions, many open vent basaltic volcanoes exhibit persistent degassing (Andres and Kasgnoc, 1998, Aiuppa et al., 2008, Burton et al., 2000, Burton et al., 2013, Carn et al., 2017, Girona et al., 2015,), which is poorly understood. Persistent degassing

has been linked to magma convection in the conduit, whereby gas-rich magma rises and outgasses, then denser, gas-poor magma sinks back down the conduit, supplying gas to the atmosphere without eruption of magma (Francis et al., 1993, Allard et al., 1994, Kazahaya et al., 1994, Stevenson and Blake 1998, Burton et al., 2007b, Huppert and Hallworth., 2007, Beckett et al., 2014). The rate of magma convection for Stromboli, for example, has been proposed to range from 300-1300 $kg \cdot s^{-1}$ (Harris and Stevenson, 1997), to account for the flux of magmatic gases emitted from the volcano (Allard et al., 1994). The style of magma flow in the conduit may be described either as Poiseuille flow (steady, axisymmetric flow through a pipe) or, if the conduit is inclined, bubbly magma will ascend along the upper wall and degassed magma back down along the lower wall (James et al., 2004); or as the ascent of undegassed magma spheres through stagnant, degassed magma (Koyaguchi, 1985, 1987, Kazahaya et al., 1994). In order to sustain surface degassing continuously for long timescales (e.g. over 10^3 years at Stromboli Volcano), a continuous input of new volatile-rich magma is required to be supplied to the shallow plumbing system (Francis et al., 1993; Allard et al., 2005, Burton et al., 2007b, Girona et al., 2015,).

Typical models of magma convection in a conduit are simplified models of two-phase exchange flows, in which melt is assumed to rise to a specific depth, degas and then return to a deeper reservoir. In practice, convection processes will be more complex due to crystallisation and the exsolution of gas from melt during magma ascent. An increase in magma crystallinity can dramatically affect the rheological properties of the ascending magma and therefore, also influence eruption style (Sparks, 1978, Belien et al., 2010, Cimarelli, et al., 2011, Oppenheimer et al., 2015, Barth et al., 2019). The presence of a crystal phase in a liquid may strongly influence the mobility of bubbles, as shown in recent studies involving three-phase analogue experiments (Belien et al., 2010; Oppenheimer et al., 2015, 2020, Barth et al., 2019). In a densely packed suspension, outgassing occurs as bursts or puffs because the granular network in the particle pack resists bubble growth and instead promotes bubble coalescence and the formation of permeable pathways (Oppenheimer et al. 2015). Similar experimental results were presented by Barth et al. (2019), who proposed that the episodic gas release during Strombolian eruptions occurs because crystalline mush in the shallow plumbing system acts as a valve to control a continuous gas supply. In their model, the size of the gas pocket depends on the overpressure within the bubble prior to the tensile failure of the particle-rich suspension. These experiments provide new insights into the mechanisms linking degassing cyclicity to the presence of crystals. Numerical simulations performed by Parmigiani

et al., (2014, 2016, 2017) focusses on the interaction between bubbles and crystals at a pore scale. In their simulations, bubbles accumulate in the magma until they overcome the capillary pressure within the pores in the crystalline magma, which promotes bubble coalescence. Additionally, the authors propose that the bubble transport dynamics changes with increasing crystal volume fraction: from suspension and channel formation to the arrest of bubbles. In analogue experiments, Pistone et al., (2017) observed that at high crystal fractions, gas exsolution can generate sufficient overpressure to form microfractures in the magma. Spina et al, (2019 b) illustrated the strong control of crystallinity on gas permeability and mobility in analogue magmas in a series of experiments.

Yasur magmas typically contain > 30 vol. % crystals (Metrich et al., 2011) and thus is an ideal natural laboratory to study the effect of the crystal phase on degassing dynamics. In this paper, we present the results of a field campaign to measure the flux and composition of volcanic gases emitted from Yasur Volcano (Vanuatu) in July 2018. We quantify gas chemistry changes over timescales of seconds during small-scale Strombolian activity, passive degassing, and recharge periods, and relate the gas composition to degassing mechanisms (e.g. 'open' vs 'closed' degassing and depth of gas-melt decoupling). We analyse high frequency time-series of Yasur's emitted plume composition and flux collected by open-path Fourier transformed infrared spectrometer (OP-FTIR) and multicomponent volcanic gas analyser (MultiGAS) and calculate gas and magma fluxes based on measurements by Ilanko et al., 2020. We also correlate several hours of video footage with the corresponding gas data to elucidate differences in gas composition associated with explosion and outgassing dynamics. This footage was used to document morphological changes in the crater and to count the frequency of bubble bursts. We use a previously published degassing model based on melt inclusion data (Metrich et al., 2011) to reconstruct volatile partitioning into an exsolved phase during magma ascent from 200 MPa to the surface, and incorporate the effect of crystallization in the shallow conduit. We use the observed CO_2/SO_2 ratio combined with melt inclusion systematics to infer the primary minimum melt CO_2 content of the Yasur melts. These model results are compared with our surface gas measurements to infer the mixing (coalescence) processes and approximate depths of gas-melt separation for different modes of outgassing with the aim to better understand Yasur's shallow plumbing system. We consider whether the high crystallinity of Yasur's magma influences the outgassing style.

2. Geological setting

Mount Yasur Volcano (361 m a.s.l) is a basaltic-andesitic volcano on Tanna island, in the archipelago of Vanuatu in the Southwest Pacific Ocean (**figure 1**). Tanna is located in the central part of the New Hebrides Island Arc and approximately 150 km above the Benioff zone caused by the subduction of the Indo-Australian underneath the Pacific plate (Carney and Macfarlane, 1979; Louat et al., 1988, Bani and Lardy, 2007, Spina et al., 2016,). The convergence rate varies from 90-120 mm per year and is controlled by the dynamics of the subduction zone and the back-arc North-Fiji basin (Taylor et al., 1995, Vergniolle and Metrich, 2016). Yasur has two summit craters, named North and South crater. Previous studies refer to three active vents (A, B, C) (e.g. Bani et al., 2013) but locals reported the permanent existence of four vents named Kraesun (South Crater, vent B in Bani et al., 2013), Wei Wei (South Crater, vent A in Bani et al., 2013), Kaunaung (North Crater, vent C in Bani et al., 2013) and Kasmiren (North Crater, vent C in Bani et al., 2013). The volcano exhibits long-lived, persistent degassing, which may have been maintained over the last 1400 years (Metrich et al., 2011, Vergniolle and Metrich, 2016), with sporadic Strombolian activity (Oppenheimer et al., 2006, Bani et al., 2013, Gaudin et al., 2014, Battaglia et al., 2016, Vergniolle and Metrich, 2016).

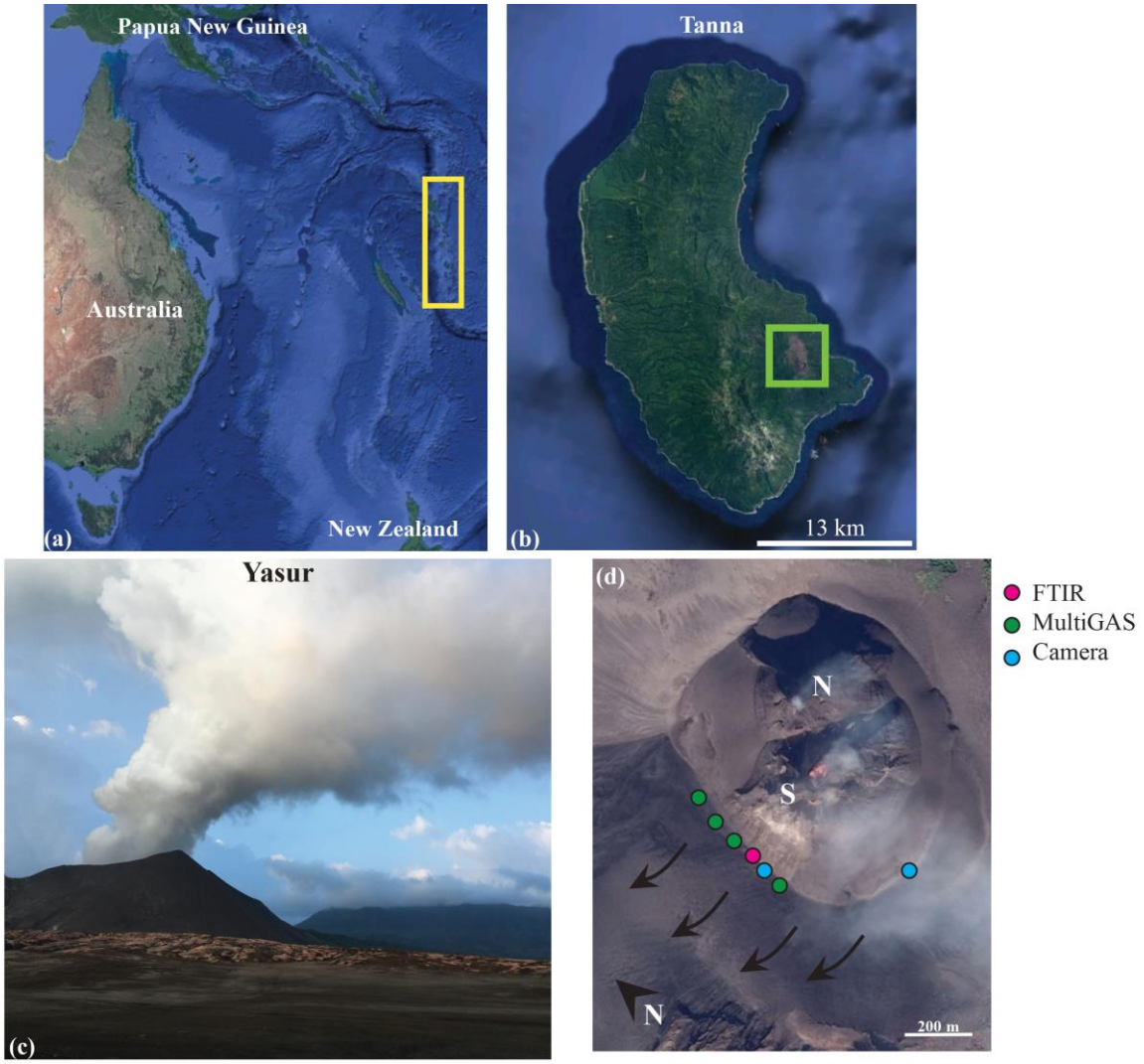

Figure 1 (a) Location of Vanuatu in the southwestern Pacific (yellow rectangle (b) Tanna island with Yasur located in the eastern part of the island (green rectangle),(c) Yasur Volcano, one of the most active volcanoes in Vanuatu and the world,(d) bird's eye view of North (N) and South (S) crater of Yasur with the position of the equipment along the crater rim pointing into the South crater: FTIR (red circle), MultiGAS (green circle) and cameras (blue circle). The arrows pointing in the west showing the prevailing plume direction.

Previous studies of volcanic outgassing at Yasur combined a high-speed thermal camera with an infrasonic sensor (Spina et al., 2016) and distinguished between two explosion classes in the South crater based on distinct spectral features and waveforms: minor explosions caused by small and continuously-bursting over-pressurised gas bubbles; and larger events, characterized as Strombolian eruptions. According to Spina et al. (2016), these kinds of eruptive events are decoupled and represent distinct mechanisms of degassing. Another classification of Yasur's explosions in both North and South crater (Meier et al., 2016) based on a multi-parametric dataset of doppler radar, infrared imagery, and infrasound, categorised

two explosion styles: ash-rich, and ash-free. A classification based solely on infrared thermal imaging in the South crater (Bani et al., 2013) differentiates between low and high energy events, and suggests that low-energy events originate in the shallow conduit, whereas the high energy events originate deeper and are associated with the bursting of slugs. Seismic (LP events) reveal that Strombolian activity is associated with signals originating at 700 – 1200 m below the summit (Battaglia et al., 2016). Oppenheimer et al (2006) identified, using OP-FTIR measurements, variations in the SO_2/HCl molar ratio between 'passive' (degassing between explosions) and 'active' degassing (Strombolian eruptions) in the South crater. Gases emitted during Strombolian explosions at Yasur in 2005 were characterised by molar SO_2/HCl ratios of up to 30 whereas those associated with passive degassing had a typical ratio between about 1.5 and 2.5 (Oppenheimer et al., 2006). The differences in the SO_2/HCl ratio were explained using two gas sources: a gas rich in SO_2, sourced at a greater depth where larger gas slugs are formed, and the shallower source rich in HCl and responsible for passive degassing (Oppenheimer et al., 2006).

Studies quantifying the volatile contents of melt inclusions (H_2O, CO_2, S, Cl) combined with MELTS modelling (Ghiorso and Sack, 1995) have suggested that extensive degassing of the melt begins at 4 or 5 km beneath the surface at Yasur (Metrich et al., 2011). In this part of the plumbing system, the basaltic-trachyandesitic magma crystallizes extensively (by > 30 vol. %), predominantly forming plagioclase feldspar (Metrich et al., 2011).

Ground-based gas measurements in October 2007 revealed that Yasur was emitting > 155 $kg{\cdot}s^{-1}$ H_2O, 7.9 $kg{\cdot}s^{-1}$ of SO_2, 9.7 $kg{\cdot}s^{-1}$ CO_2, 1.9 $kg{\cdot}s^{-1}$ HCl and 0.3 $kg{\cdot}s^{-1}$ HF (Metrich et al., 2011). The SO_2 emission rate derived from satellite-based Ozone Mapping Instrument (OMI) measurements from 2000 to 2015 averaged 16.3 $kg{\cdot}s^{-1}$ (Carn et al., 2017). As a result, Yasur ranks at number 11 in a list of 91 degassing volcanic SO_2 sources (Carn et al., 2017). SO_2 flux measurements during field campaigns in 2004, 2005 and 2007 reveals fluxes ranging from 1.9 to 14.5 $kg{\cdot}s^{-1}$ SO_2 in 2004 and 2005 (Bani and Lardi, 2007) and 7.9 ± 3.8 $kg{\cdot}s^{-1}$ SO_2 in 2007 (Metrich et al., 2011).

3. Methods

Volcanic gas composition and flux measurements were carried out on Yasur Volcano from 6 to 16 July 2018 using an open path Fourier transform infrared spectrometer (OP-FTIR), Multi-

GAS and UV cameras (**figure 1**). On 16 July, a MIDAC M4410-S FTIR spectrometer fitted with a ZnSe beam splitter and a Stirling engine-cooled detector was deployed on the southern crater rim (location shown on **figure 1e**), powered by a 20 Ah battery. A laptop running AutoQuant Pro 4.5 software, connected to the FTIR, controlled data acquisition. The spectrometer was placed on a tripod and positioned to collect infrared radiation from a hot vent in the South crater (**figure 1**). The nominal field of view of the spectrometer is 20 mrad. The distance between the infrared source and the spectrometer was approximately 300 m. The volcanic gases from the multiple different vents mixed inside the crater, such that measurements of gases from only one particular vent was not possible. Analysis of FTIR spectra is based on the principles of absorption spectroscopy. We used the HITRAN database 2008, which provides the absorption coefficients (Rothman et al., 2009).

Spectra were acquired during the following intervals (in GMT time): 06:41-06:56 h (set 1), 08:19-08:24 h (set 2) and 08:56-09:03 (set 3). All interferograms were collected at a time step of 1 second and a nominal 0.5 cm^{-1} spectral resolution. In total 698 spectra were collected. Column amounts of SO_2, and HCl were retrieved from single beam spectra using a code that simulates and fits atmospheric transmittance in discrete wavebands (Burton et al., 2000). The code gives for each selected gas a 'goodness of fit', which provide information about how close the computed and the measured spectra fit. The average fitting error for SO_2 is 4.8 % (standard deviation of the average error, sd: ± 0.63 %) and 6.9 % (sd: ± 0.86 %) for HCl. Laboratory experiments were carried out in previous studies to validate the precision of the measurements using primary gas standards, suggesting accuracies of order of 5 % for retrieved column amounts of SO_2 and CO (Horrocks et al., 2001,). The wavebands selected to retrieve volcanic gas species were: 2020 to 2100 cm^{-1} for H_2O and CO_2, 2430 to 2530 cm^{-1} for SO_2 and 2680 to 2835 cm^{-1} for HCl. The uncertainty on FTIR gas ratios was calculated by propagating the errors on individual retrievals i.e. the root of the sum of the individual maximum fitting errors. The maximum fitting error for SO_2 was of 8.7 % and for HCl is was of 10.4 %. Therefore, the calculated error for this SO_2/HCl ratio is 14 %.

A multicomponent gas analyser system (MultiGAS; Aiuppa et al., 2005, 2010, Shinohara, 2005) was used to measure the composition of the volcanic plume (sourced from both, the North and South crater; **figure 1e**) from 6 to 16 July 2018. The Multi-GAS hosts infrared sensors (LI-840 NDIR closed-path spectrometer, measurement range 0-3000 ppmv for CO_2 accuracy, ± 1.5 %), and electrochemical sensors (model 3ST/F, Cod.TD2D-1A,City

Technology Ltd., calibration range, 0–30 ppmv; repeatability 1%) for SO_2. The infrared and the electrochemical sensors are protected by a pelican case and the volcanic plume is pumped at a rate of 0.6 L min^{-1} to the sensors. The sensors are connected to a data logger that is programmed to capture measurements of the plume at a sampling rate of 1 Hz (Aiuppa et al., 2010). The Multi-GAS was placed at the southern and western rim of Yasur (**figure 1e**) and powered by lithium battery. It measured the concentration of the volcanic gases by integrating the infrared sensor for CO_2, the electrochemical sensors for SO_2 and temperature, pressure and relative humidity of H_2O. MultiGAS time series were post-processed by using the Ratiocalc software (Tamburello et al., 2015). Uncertainties in derived molar ratios, based on laboratory test results are, for CO_2/SO_2 with $SO_2 > 0.16$ mol, ± 6 % and with $SO_2 < 0.16$ mol the error increases to ± 12% (Liu et al., 2019). Errors for H_2O/SO_2 ratios, based on laboratory tests, are ± 25%. For this study, we obtained 7523 measurements.

Ultraviolet (UV) cameras (PiCam; Wilkes et al., 2016; 2017) were used to measure the emission rate of SO_2 during the same time period (the methods and full results are described and presented in Ilanko et al.,2020). The method is based on the characteristic absorption of scattered UV sunlight by SO_2 between 300 and 320 nm (Mori and Burton, 2006, Kantzas et al., 2010, Kern et al., 2015). SO_2 emission rates derived from the PiCam data in the period of 6^{th} to 9^{th} July 2018 were used to derive fluxes of the other gas species (Ilanko et al., 2020). The calculated error for the HCl flux is 21 % based on propagating errors from the SO_2 flux measurement (~ 15 %, Ilanko et al., 2020) and error on molar SO_2/HCl (from FTIR).

Lastly, videos and photos captured eruptive activity enabling recording of gas burst frequency, changes in crater morphology and volcanological features of the crater and vents during the period of the field work, using a 12 MP camera at 60 fps (iphone SE). To compare the activity between the North and South craters, a 12 MP camera at 240 fps (go pro hero 7) was installed at the eastern rim to overlook the North and South craters. Both camera positions in figure 1c were used to acquire video images for counting bubble bursts.

4. Results

4.1 Video observations of the South crater

The number of active vents in the South crater emitting gas and/or magma during the fieldwork varied from 5 to 7 (**figure 2**). Six vents were observed on 9 July (**figure 2a**), 7 on 11 July (**figure 2b**), 6 on 13 July (**figure 2c**) and 5 on 15 and 16 July (**figure 2d**). The two principal vents (vent 1 and 2 in figure 2) did not change their position during the field period whereas other minor vents changed their positions and sizes or appeared and disappeared from day to day. Video observations reveal that small bubble bursts generated ejecta that rose a few tens of metres above the vents whereas larger bubble-bursting events generated bombs that were expelled to a height of > 10 metres above the vents and landed outside the crater. The overall number of large bubble bursts which were counted on the video (and generated ejecta) per second was 4 ± 0.1 s^{-1} on 9 July, 1.3 ± 0.3 s^{-1} on 11 July, 0.8 ± 0.3 s^{-1} for 13 July in the morning and 0.7 ± 0.3 s^{-1} in the evening and 1.3 ± 0.1 s^{-1} for 15 and 16 July. Table 1 shows the overall number of bubbles which were observed in different vents of figure 2. The average time interval between large bubble bursts (Strombolian explosions) from 8 to 16 July was 54 (± 44) seconds i.e. 0.02 large bubble bursts s^{-1}. One of the principal vents exhibited a consistent style of volcanic activity throughout the measurement period, characterised by Strombolian explosions, which expelled volcanic bombs that occasionally reached the crater rim and were sometimes accompanied by shock waves. The second principal vent showed a different behaviour, exhibiting jet-like gas emission after the bursts that lasted for several seconds. These Strombolian explosions ejected volcanic bombs several hundred meters into the air and were accompanied by shock waves. All the other vents were less active, erupting only a little material (via spattering).

Table 1. Calculated bubble bursts per s^{-1} from vents at Yasur Volcano, Vanuatu in July 2018. The location of the vents are shown in figure 2 over different days. Each calculation is based on 224 to 776 seconds worth of video data.

day	Bubble bursts per second						
	Vent 1	Vent 2	Vent 3	Vent 4	Vent 5	Vent 6	Vent 7
9th July	0.01	0.05		0.06	0.02		
11th July	0.009	0.03	0.40		0.29		0.018
13th July	0.003	0.17	0.43	0.16	0.45	0.01	
15th/16th July	0.009	0.36	0.26	0.26	0.36		

4.2 Volcanic plume composition from MultiGAS

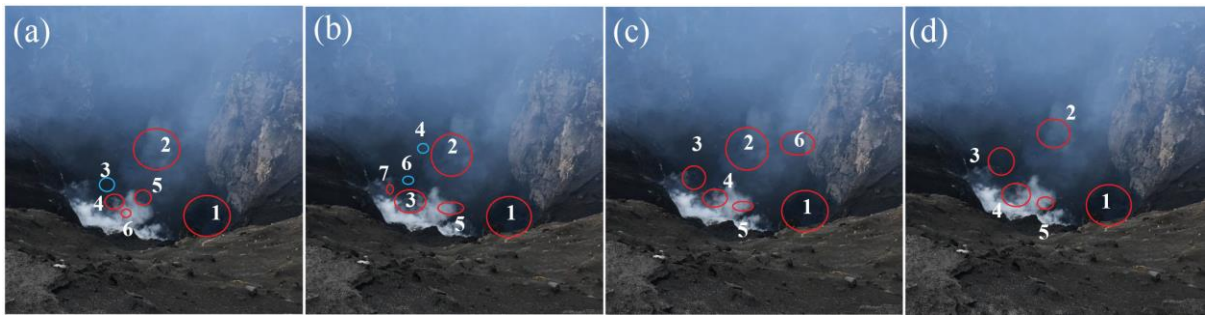

Figure 2 Vent location in the crater of Yasur Volcano, Vanuatu, on (a) 9th July, (b) 11th July, (c) 13th July and (d) 15th - 16th July 2018. Estimated field of view is between 200 and 300 m.

MultiGAS results are shown in **figure 3** and **table 2**. Across all days, the mean gas concentrations varied between 17.7 and 25.4 ppm CO_2, 14.1 to 14.8 ppm SO_2 and 364 to 854 ppm H_2O. The mean volcanic gas concentrations in the plume across all four days is: 22.2 ppm CO_2, 14.4 ppm SO_2 and 610 ppm H_2O. The mean molar plume composition for all four days is 97.9 mol % H_2O, 1.44 mol % CO_2 and 0.66 mol % SO_2.

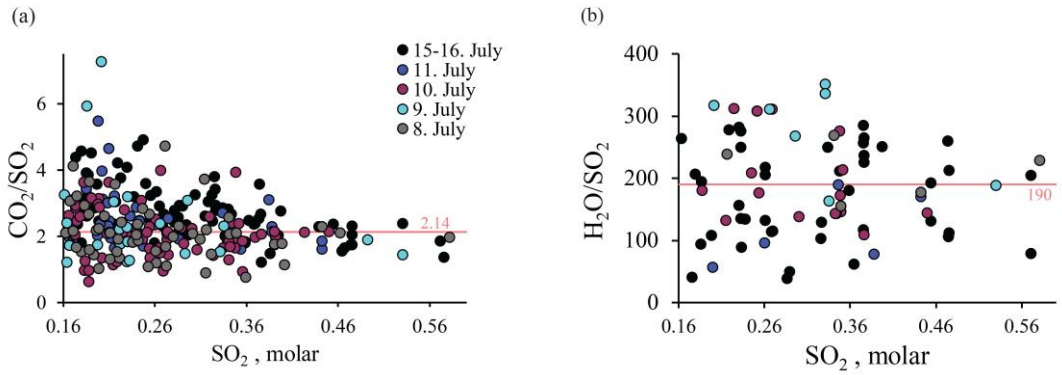

Figure 3 Scatter plots of Yasur Volcano's plume gas emissions for 8th to 16th July: (a) Molar CO_2/SO_2 vs. SO_2 and (b) Molar H_2O/SO_2 vs. SO_2, with the average value of CO_2/SO_2 and H_2O/SO_2 ratios (with SO_2>0.3) marked as a horizontal line, marked with value. Each point corresponds in (a) to a CO_2/SO_2 and in (b) to a H_2O/SO_2 peak in the measured data set (CO_2/SO_2: 315 data points, H_2O/SO_2: 86 data points). Below SO_2 concentrations of 0.16 mol% the error increases from ± 6 to ± 12%.

Table 2 shows the mean molar CO_2/SO_2 plume ratios for all days, which ranged from 1.80 on 9 July to 2.48 on 16 July. **Figure 3a** shows CO_2/SO_2 ratios plotted against SO_2 for single eruption gas peaks recorded in the volcanic plume for each day and shows that CO_2/SO_2 were consistent from day to day, converging on an overall mean of 2.14 for molar SO_2 values > 0.16

(there is a larger spread at lower SO_2 values; **figure 3a**). The daily molar H_2O/SO_2 plume ratios (**table 2**; **figure 3b**) are highly variable, ranging from a mean of 89.3 ± 22.3 for 11 July and 205 ± 51.3 for 16 July with a mean value of 190 for molar SO_2 values > 0.3 mol %, although there is considerable scatter (**figure 3b**). This variability in molar H_2O/SO_2 is linked strongly to degassing regime: low H_2O/SO_2 is associated with powerful Strombolian eruptions (**figure 4a-d**).

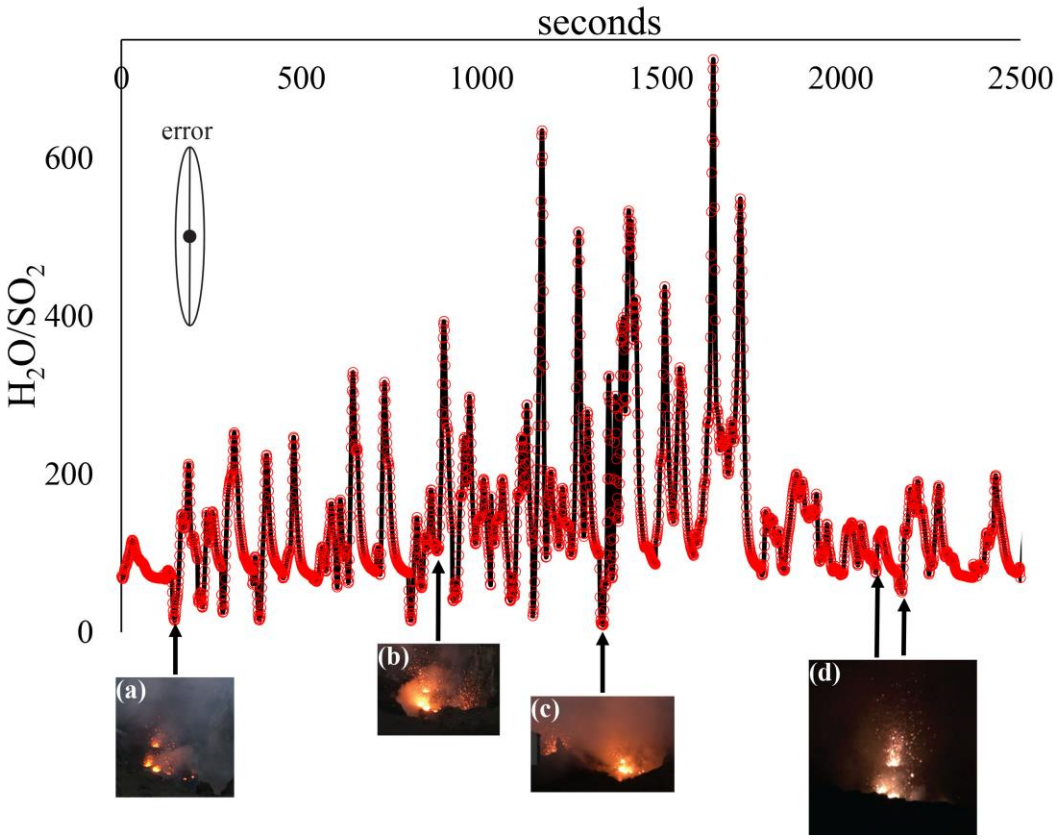

Figure 4 H_2O/SO_2 ratio for a Multi-GAS measurement period on 16th July from 5:22 to 6:45 pm. Photos from (a) to (d) show the prevailing different eruption styles in North and South crater: (a, d): spattering activity in the Southern crater, (b) spattering and a mild strombolian eruption in the South crater and (c) mild strombolian eruption in the South crater and powerful strombolian eruption in the North crater. Both, the H_2O and the SO_2 content of the volcanic gases increases from spattering over mild to powerful strombolian eruptions. Eruptive events occur on average every 62 (sd: 30) seconds.

*Table 2: Composition of Yasur Volcano's volcanic gas plume measured by MultiGAS on for 9, 10, 11, and 16 July 2018. n: number of measurements including data measurements with SO_2 < 0.16 mol, *mean concentration, in ppm (standard deviation), $molar percentage of each component, ^molar ratios.*

		16 July	*11 July*	*10 July*	*9 July*	*Mean*
	n	4809	959	1280	475	
**Mean concentration*	CO_2	25.4 (10.1)	23.3 (8.0)	22.2 (7.1)	17.7(102)	22.2
	SO_2	14.8 (4.9)	14.4 (3.9)	14.1(3.3)	14.4 (5.3)	14.4
	H_2O	854 (274)	364 (276)	747 (289)	474 (389)	610
$Molar composition, %	H_2O	98.3	96.4	98.3	97.7	97.9
	CO_2	1.20	2.53	1.18	1.49	1.44
	SO_2	0.48	1.10	0.52	0.82	0.66
^Molar ratios	CO_2/ SO_2	2.48	2.33	2.31	1.80	2.22
	H_2O/ SO_2	205	89.3	189	118	148
	H_2O/CO_2	82.6	38.3	81.9	65.6	61.1

4.3 Volcanic gas composition from OP-FTIR spectroscopy

Figure 5 shows the retrieved column amounts for HCl, CO_2, and SO_2 from the time series of set 1 from the South crater, which was obtained from the southern crater rim. The record identifies 16 explosions in 360 s (identified by the rapid increase in gas column amounts) and provides information about changes in gas ratios before and during explosions. We differentiate between active degassing, consisting of intermittent Strombolian explosions and spattering; and passive degassing.

A cyclicity is visible when less active periods are interrupted by explosions, identified by an increase in SO_2 and CO_2 followed by a decrease (**figure 5**); explosions occur at the peaks of these cycles. In set 1, explosions 1, 2 and 3 were accompanied by a rise in SO_2 column amounts, followed by a decrease to pre-explosion column amounts of SO_2 after ~ 60 seconds. Smaller explosions (4, 5, 7, 9, 10, 11, 13, and 16; **figure 5**) are associated with peaks in SO_2 column amounts up to $<4.93 \cdot 10^{19}$ molecules·cm^{-2} after which SO_2 column amounts remain elevated above the pre-explosion level. Explosions 6 and 8 were associated with increases in SO_2 column amounts up to $5.26 \cdot 10^{19}$ and $7.07 \cdot 10^{19}$ molecules·cm^{-2} respectively, which then decreased after the explosions, returning to pre-explosion values after ~20 seconds. Variation in the concentration-pathlengths of the measured gases could be also caused by the dilution effect of wind gusts in the crater but we regard it unlikely as these changes occur periodically, which is more consistent with the observed volcanic activity.

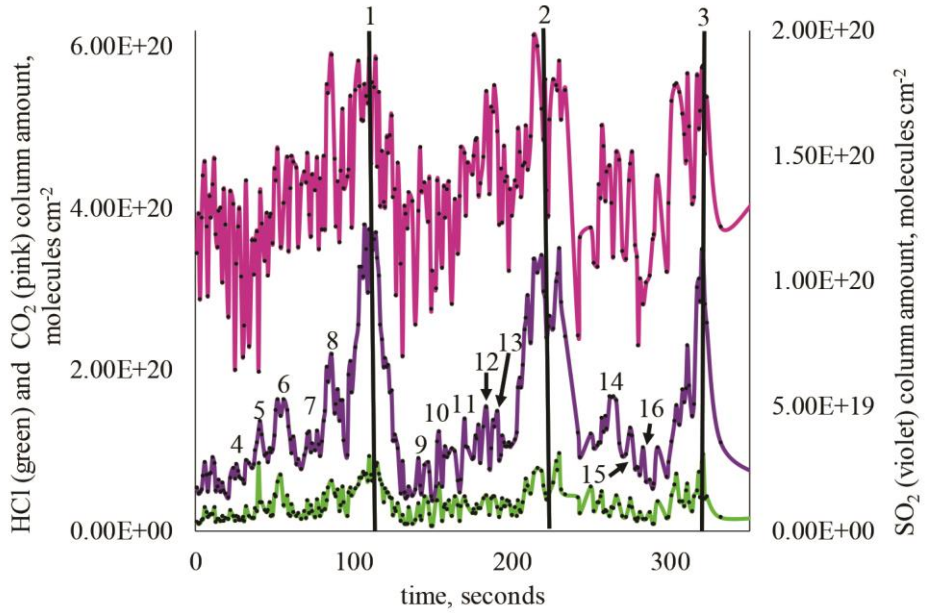

Figure 5 Time-series of retrieved column amounts of HCl (green), SO_2 (violet), CO_2 (red) for data set 1, in molecules·cm^{-2}. Prominent strombolian explosions are numbered with 1, 2, 3 and occur ~every 100 seconds. Numbered peaks from 4 to 16 mark minor explosive events prior to the strombolian events.

We observe that active degassing from the South crater is distinguished by a molar SO_2/HCl ratio between 1 and 1.7 (**table 3, figure 6**); whereas a SO_2/HCl < 1, where HCl is dominant compared to SO_2 in the gas phase, characterises the passive degassing periods (**table 3, figure 6**). In 2005, Strombolian eruptions in the South crater emitted gas with molar SO_2/HCl >30, and passive degassing was characterised by molar SO_2/HCl between 1.5 and 2.5 (Oppenheimer et al., 2006). Photos taken in 2005 revealed more violent eruptions occupying the whole crater and with a higher number of volcanic pyroclasts, ejected to greater heights (Oppenheimer et al., 2006). This violent type of eruption was not observed in July 2018. The composition of volcanic gases during active and passive phases is shown in **table 3**.

*Table 3: Mean chemical composition (as molar ratios) of volcanic gases emitted from Yasur Volcano, Vanuatu, during 'active' and 'passive' (non-explosive) phases on 16 July 2019. *South crater measured by OP-FTIR ; $^{+}$Plume of North and South crater measured by MultiGAS. Uncertainties on the mean molar ratios are shown as a ± range. Number of measurements in each case are shown in brackets.*

Molar ratio	*Active phase*	*Passive phase*
$^{+}H_2O/SO_2$	315 ± 78.8 (222)	174 ± 43.5 (477)
$^{+}CO_2/SO_2$	2.85 ± 0.17 (222)	1.96± 0.12 (477)
$^{*}SO_2$/HCl	1.6 ± 0. 22 (84)	0.5 ± 0.07 (423)

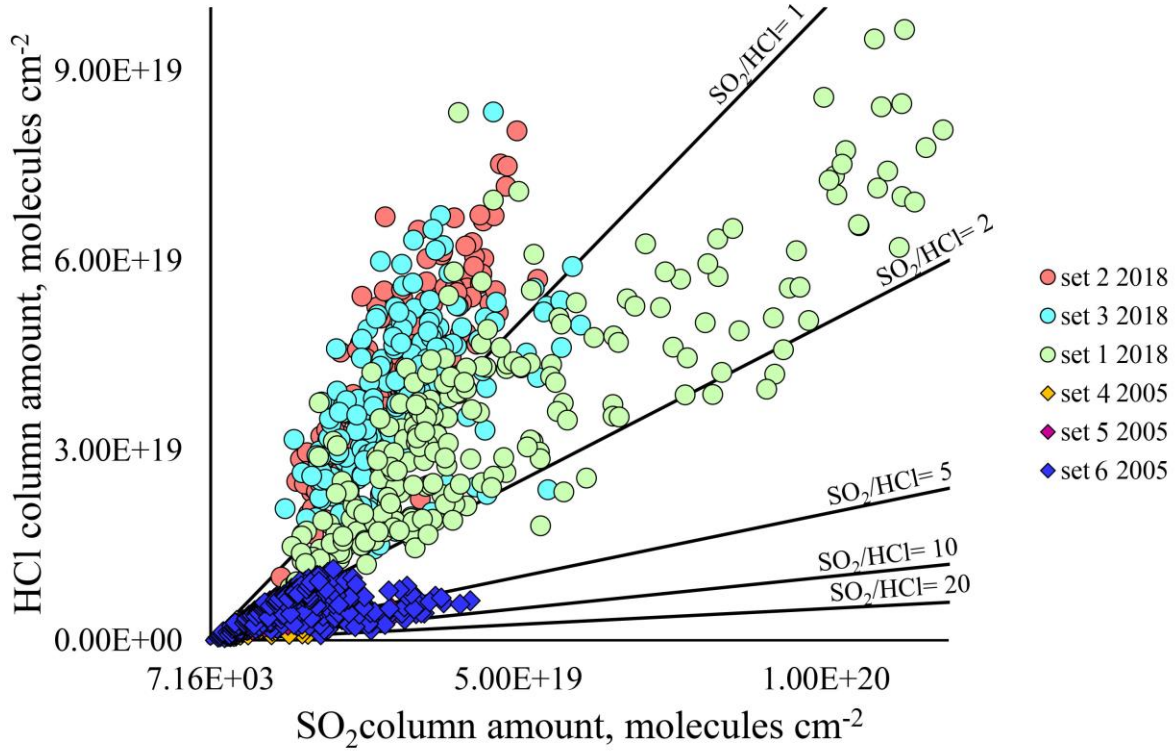

Figure 6 Column amounts for SO_2 and HCl for spectra from set 1 (green circles; 06:41-06:56 h), set 2 (red circles;08:19-08:24 h) set 3 (blue circles; 08:56-09:03 h) measured all from the same position on the South crater on 16 July 2018 and data from the South crater on 1 January 2005 including set 4(yellow diamonds: 09:19-09:22 h), set 5 (pink diamonds: 09.23-09.24 h) and set 6 (blue diamonds: 09:24-.09:25 h) (Oppenheimer et al., 2006). Solid lines indicate the SO_2/HCl ratios. Passive degassing is characterised by HCl>SO_2 whereas active degassing has higher SO_2 concentrations (SO_2> HCl). Higher ratios indicate a higher proportion of explosive gas. Set 1 is compared to set 2 and set 3 a period of higher activity. (Average HCl error: ± 7 % and SO_2 error: ± 4.8 %).

4.4 Volcanic gas fluxes

In **table 4** we show the flux of SO_2, CO_2 and HCl from Yasur Volcano in 2018, derived from UV camera data (Ilanko et al., 2020) and from the Multi-GAS and FTIR molar ratios (**table 2**) compared to those of other basaltic open vent volcanoes known for their Strombolian activity. The mean SO_2 flux has been measured as 7.9 kg·s^{-1} (Bani and Lardi, 2007), 7.9 kg·s^{-1}(Metrich et al., 2011) and 4.9 kg s^{-1} used in this study (Ilanko et al., 2020).

Combining the flux measured in 2018 with the mean mass ratios in the gas plume (**table 2** and the average SO_2/HCl value of 1.02) we calculate daily fluxes of 7.5 kg·s^{-1} CO_2 (± 16.2 %), 208 kg·s^{-1} H_2O (± 29.2%) and 4.8 kg·s^{-1} HCl (± 13.6%). In 2007 the corresponding fluxes were 9.7 kg·s^{-1} CO_2 (29 % higher than in 2018), the HCl flux was 1.9 kg·s^{-1} (60 % lower than in 2018) and the SO_2 flux was 7.9 kg·s^{-1} (61 % higher than in 2018). We compare the active and passive

CO_2/SO_2 and SO_2/HCl ratios with the overall mean ratios in order to get an estimate of the amount of gas supplied by active rather than passive degassing. For example, the mean molar CO_2/SO_2 is 2.14 and the gases emitted during active degassing periods have a CO_2/SO_2 of 2.85 and the passive degassing periods 1.96. Active degassing therefore provides 20% of the total gas flux. The same value (20%) is derived using the overall mean molar CO_2/SO_2 of 2.14 and the active and passive degassing ratios (2.85 and 1.96). An SO_2 flux of 4.9 ± 0.74 $kg \cdot s^{-1}$ is the same as 423 ± 63 tonnes of SO_2 per day, of which only ~ 85 tonnes per day is derived from active degassing, the rest passive degassing. Using a bubble burst frequency of every 0.02 seconds; we infer a bubble volume of 14250 m^3.

Table 4: Average volcanic gas composition (molar ratios) and fluxes (in $kg \cdot s^{-1}$) emitted from Yasur Volcano, Vanuatu, in July 2018 Stromboli (Italy), Villarrica (Chile) and Masaya (Nicaragua).

		Yasur, Vanuatu	*Stromboli, Italy*	*Villarrica, Chile*	*Masaya, Nicaragua*
Molar ratios	CO_2/SO_2	2.22 ± 0.13 [a]	5.7 [c] ± 0.34 - 8 [g] ± 0.48	1.5 [e] ± 0.09 1.7 [e] ± 0.11	2.7 ± 0.3 [f]
	H_2O/SO_2	148 ± 48 [a]	26.7 [c] ± 6.7 - 48.8 [g] ± 5.7	67 [e] ± 16.8- 75 [e] ± 18.8	63±7 [f]
	SO_2/HCl	1.0 ± 0.14 [a]	1.00 [h] ± 0.08 - 1.50 [h] ± 0.12	3 ± 0.1 [i]	2 ± 0.03 [f]
Mass fluxes	SO_2	4.9 ± 0.74 [b]	0.7 [d] ± 0.12 - 3.0 ± 0.45 [g]	1.5 [e] ± 0.18- 3.7 [i] ± 0.56	7.9 ± 2.37 [f]
	HCl	4.8 ± 1.01 [a]	0.4 [d,h]-1.1 [g,h]	0.3 [e,i]-0.7 [i]	2.2 [f]
	CO_2	7.5 ± 1.20 [a]	2.6 [c]-d-15.8 [h],	1.5 [e]-4.1 [i]	13.9 [f]
	H_2O	208 [a]	5.2 [c,d]-41.2 [h]	28.3 [e]- 78.0 [e,i]	140 [f]
	Total gas	225	8.9-61.1	31.6-86.5	164

[a] This study: average composition 2018; [b] Ilanko et al., 2020, [c] Aiuppa et al., 2010, [d] Tamburello et al., 2012, [e] Liu et al., 2018, [f] Martin et al., 2010. [g]Allard ,2010, [h] Burton et al., 2007, [i] Sawyer et al., 2011,

5. Discussion

5.1. Gas evolution and outgassing in a crystal-rich conduit

We use geochemical data from Yasur's primitive melt inclusions in olivines (Metrich et al., 2011) to generate a model of closed system magma degassing and compare it with the measured gas composition at the surface (**table 3**) to infer the approximate pressure of last gas-melt equilibration, which may be equivalent to the gas segregation pressure, for active and passive modes of degassing. Extensive petrological study of Yasur magmas has led to a model (**figure 7; table 5**) whereby primitive basaltic magmas enter the system at depths of > 6 km containing ~2500 ppm CO_2 (reconstructed from melt inclusion data and volcanic gas ratios; Metrich et al., 2011), ~ 1 wt% H_2O, 0.1 wt% S and ~550 ppm Cl. We use the S contents of the melt inclusions and the mean CO_2/SO_2 of the gas plume in 2018 to estimate a 'primary' (pre-degassing) melt CO_2 content. Using an average sulfur content of melt inclusions of 0.1 wt. % (Metrich et al., 2011) and the average CO_2/SO_2 plume mass ratio of 1.5 in July 2018, we obtain a pre-degassing bulk melt CO_2 content of 3000 ppm, assuming complete degassing of sulfur and CO_2 on eruption, compared with 2500 ppm estimated by Metrich et al. (2011) using the same method.

At pressures between 330 and 130 MPa, the exsolved volatile phase is comprised almost entirely of CO_2 (resulting in the molar CO_2/SO_2 going to infinity at pressures >130 MPa in **figure 7**). The primitive basalt undergoes extensive crystallisation in a magma reservoir between 130 and 50 MPa (melt fraction remaining ~ 0.46) to produce basaltic-trachyandesite (Metrich et al., 2011). Olivine-hosted melt inclusions of basaltic-trachyandesite that are assumed to have originated in this reservoir contain up to 1 wt.% H_2O, 780 ppm S, 1200 ppm Cl and ~500 ppm CO_2 (Metrich et al., 2011). By this stage 63% of S, and 43% of bulk magmatic water content has been lost to the vapour phase. The exsolved volatile phase existing in equilibrium with the basaltic trachyandesite melt at this pressure has a molar CO_2/SO_2 of ~2.6, and molar SO_2/HCl >100 (**figure 7; table 5**).

Between 50 MPa (~ 2 km) and the surface ('stage II' of Metrich et al., 2011), S and Cl degas from the melt (**table 5; figure 7**). At the end of this stage, 29% of the Cl, 86% of the bulk S, and 90% of the bulk water has been lost from the magma (Metrich et al., 2011). The exsolved volatile phase is expected to have a molar CO_2/SO_2 of ~1.8-2.0 in this pressure interval, and a molar SO_2/HCl of 2-6 (**figure 7; table 5**). On eruption (stage III), an additional ~ 40% of Cl exsolved into a vapour phase, as well as an additional 8% S and 4% H_2O. This low pressure

gas is highly enriched in HCl, generating a molar SO_2/HCl of < 3, with a molar CO_2/SO_2 of 1.7 to 2 (**table 5; figure 7**).

Table 5 Yasur's melt composition from primitive melt inclusions (Metrich et al., 2011) and the calculated emitted amount and gas composition for degassing stage I,II, and III in a closed degassing system. The melt fraction in each stage was used to calculate the crystal fraction at each stage (1-f) and incorporate fractional crystallization in the melt degassing process.

Stage	Pressure, MPa		Melt, wt%					f, melt fraction	Amount degassed, ppm				Volcanic gas ratios, molar	
	Max	**Min**	**CO_2**	**H_2O**	**S**	**Cl**	**Comp**	**K_2O_0/K_2O**	**ΔCO_2**	**ΔH_2O**	**ΔS**	**ΔCl**	**CO_2/SO_2**	**SO_2/HCl**
	330	180	0.25	0.8	0.099	0.055	bas	1	0	0	0	0	∞	∞
I	130	110	0.05	1.2	0.078	0.1235	bas-trach-and	0.46	4934	5391	1370	10	2.6	152
II	100	50	0.005	1.2	0.033	0.091	bas-trach-and	0.43	5763	6605	1972	369	2.1	5.9
III	50	0	0.001	0.2	0.006	0.046	bas-trach-and	0.35	7132	2087	2768	1111	1.9	2.8

We compare our gas data (**table 3**) as well as previously published data (Merich et al., 2011) to the model (**figure 7)**. The gas compositions for passive degassing are consistent with gases being derived predominantly from the shallowest parts of the conduit system, at pressures of <10 MPa (depths approximately <400 m). These gases are relatively enriched in HCl and have the lowest CO_2/SO_2 values. During the 'active' degassing (Strombolian explosions and spattering), the gases become depleted in HCl and more CO_2-rich, consistent with their derivation from deeper in the conduit, perhaps down to 0.6 to 2 km depth (**figure 7**).

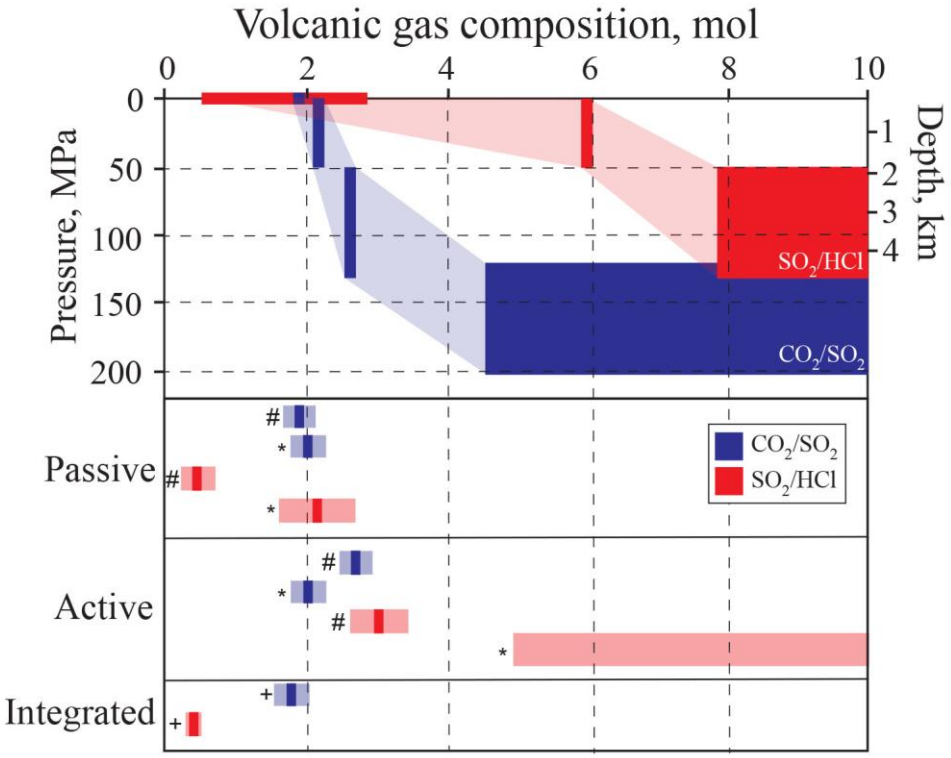

Figure 7 Predicted volcanic molar gas composition from melt inclusion data with pressure and depth for Yasur Volcano, reconstructed from melt inclusion data (Metrich et al., 2011). Molar CO_2/SO_2 is shown in blue, and molar SO_2/HCl in red. Depths are estimated using a crustal density of 2800 kg·m^{-3}. Bottom: volcanic gas compositions measured at Yasur for passive degassing, active degassing (Strombolian activity) and measurements taken integrated over both passive and active periods. S_1-S_3 stands for different stages proposed in Metrich et al., 2011. Symbols denote data source. #: this study; *: Oppenheimer et al., 2006; +: Metrich et al., 2011. The dark rectangle denotes the mean value and the light shaded rectangle the range in probable values.

Petrological studies have shown that between 6 and 1.8 km depth, the basaltic parent magma crystallises by > 46 vol. % (Metrich et al., 2011) to produce the basaltic trachyandesites that are erupted. Erupted magmas contain around 30 vol. % crystals (predominantly plagioclase phenocrysts up to 5 mm in size, and minor olivine, clinopyroxene and Fe-oxides; Metrich et al., 2011), which suggests that significant volumes of crystals (dominantly olivine) must accumulate in a subsurface mush pile. Extensive crystallisation in the upper 1-2 km of the conduit, driven by water degassing, induces changes in the rheological properties of the magma. We use the Giordano et al. (2008) viscosity model with a typical melt inclusion composition from Metrich et al. (2011) and a H_2O content of 1.1 wt% for pre-degassing and 0.2 wt. % after degassing. Based on the MELTS output the crystallinity increases from 10 to 32 vol. % on degassing. We find that the bulk magma effective viscosity increases from 5.8 x 10^2 Pa·s prior to degassing to 1.5 x 10^5 Pa·s after degassing and crystallisation.

In line with recent studies showing how the exsolved gas phase interacts with the crystal phase (Belien et al., 2010, Parmigiani et al., 2014, 2016, 2018, Oppenheimer et al., 2015,2020, Pistone et al., 2017, Barth et al., 2019, Spina et al., 2019b,), we suggest that the increase in the crystallinity and bulk viscosity of the magma creates a plug at the top of the conduit that develops an effective yield strength (figure 8). Our hypothesis is consistent with previous work: Kremers et al., (2012) suggested that a degassed, viscous plug may exist in the upper conduit of Yasur, based on the observed mingling of sideromelane and microlite-rich tachylite. We envisage Yasur's shallow conduit consisting of a crystal-rich region with a thickness of at least 0.6 and up to 2 km, if extensive crystallization is driven by H_2O degassing (Metrich et al., 2011). Magmatic gas bubbles (with a slight CO_2-enrichment over gases closer to the surface, and poor in HCl) will accumulate in the crystal-rich plug , before generating a local overpressure that is sufficient to overcome the yield strength of the overlying crystal plug **(figure 8a)**. The gas bubble will then migrate upward **(figure 8b, c)** and transport magma in its wake (Del Bello et al., 2015). At the surface, the bubble bursts as a typical Strombolian eruption with a gas phase enriched in CO_2 compared to SO_2 (**figure 8d**). The plug rebuilds and bubbles begin to get trapped again and a new cycle starts (**figure 8g**). Bubbles released during 'passive degassing are sourced from close to the surface and in general, these shallow gases are richer in HCl than the deeper accumulated gases due to the fact that HCl exsolves at pressures < 10 MPa.

5.2. Degassing rates and magma fluxes

We may calculate the net upward flux of magma in the conduit required to supply the observed fluxes of SO_2 at the surface (**table 4**). Using the maximum pre-eruptive sulphur concentrations of 1000 ppm in primitive olivine-hosted melt inclusions (Metrich et al., 2011) and mean SO_2 fluxes of 4.9 $kg \cdot s^{-1}$ measured in the time periods of 6^{th} to 9^{th} July 2018 (Ilanko et al., 2020) ,we infer a magma supply rate ~2450 $kg \cdot s^{-1}$, for a magma mean density of 2650 $kg \cdot m^{-3}$ and a crystallinity of 32 vol. %. Our calculated bulk magma degassing rate of 2450 $kg \cdot s^{-1}$ is lower than previous estimates of magma degassing rate of 4100 $kg \cdot s^{-1}$ (Metrich et al, 2011). We assume in this calculation that the magma degasses all of its sulfur (the S concentration in the erupted glass matrix is 0.006 wt.%). Yasur volcano has been degassing for the last 1400 years (Vergniolle and Metrich, 2016). Over long timescales the flux of degassing (but not necessarily erupted) magma is ~0.04 km^3 per year, with a minimum of 54 km^3 degassed magma

presumably stored as a plutonic body at depth over 1400 years, consistent with previous estimates (0.05 km^3 per year; Metrich et al., 2011).

These new data from Yasur volcano in 2018 provide insights into the influence of crystals on bubble formation events in the shallow conduit. These crystals may form a viscous plug that influences bubble formation depth and consequently their chemical fingerprint. It is known that magma in the shallow conduit of other Strombolian active volcanoes is crystal-rich, with 30 to 60 vol. %. This crystal content might be high enough to develop an effective yield strength to trap bubbles and form slugs.

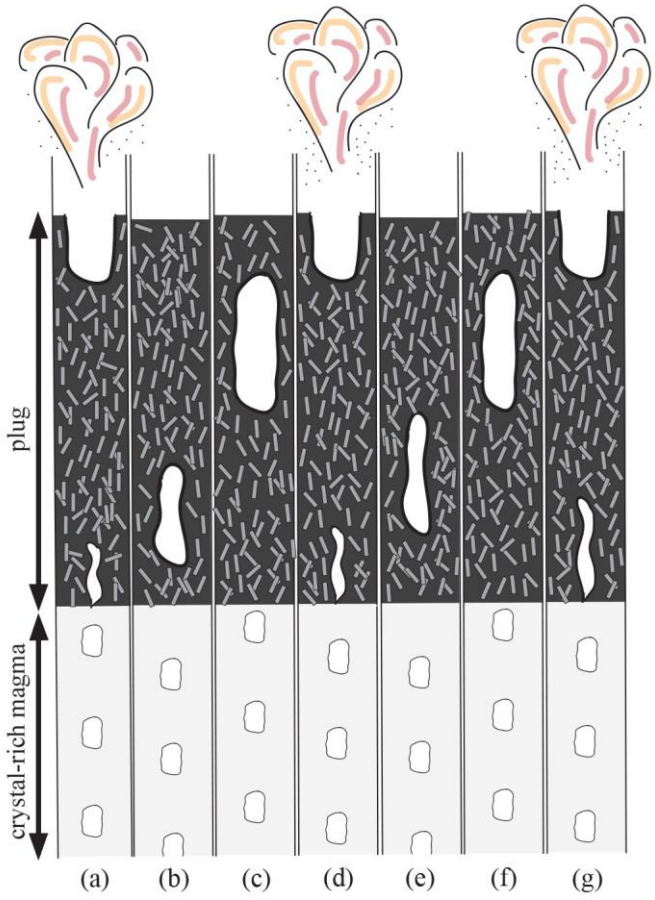

Figure 8 Schematic diagram shows the shallow plumbing system of Yasur Volcano (from 600 bar to the surface). (Described in main text).

6. Conclusions

We present volcanic gas flux and composition data from Yasur Volcano, Vanuatu, during a field campaign in July 2018. We draw the following conclusions:

(1) The average volcanic plume chemistry is characterised by a mean molar CO_2/SO_2 ratio of 2.12, H_2O/SO_2 of 148 and SO_2/HCl of 1.0. The mean SO_2 flux is 4.9 $kg \cdot s^{-1}$. Therefore, the mean fluxes of the other species are 7.5 $kg \cdot s^{-1}$ CO_2, 208 $kg \cdot s^{-1}$ H_2O and 4.8 $kg \cdot s^{-1}$ HCl.

(2) The degassing regime at Yasur Volcano, as also defined from previous studies (Oppenheimer et al., 2007; Metrich et al., 2011) ranges from 'passive' to 'active' styles, with the latter characterised by strombolian explosions. These styles are also distinguished by their characteristic gas compositions in July 2018: (a) gases emitted during active degassing are enriched in SO_2 and CO_2 with CO_2/S ratios of 2.85 ± 0.17, SO_2/HCl with 1.6 ±0.22 and H_2O/SO_2 with 315 ± 78.8 (b) passive degassing is enriched in HCl with CO_2/SO_2 ratios of 1.96 ± 0.12, SO_2/HCl with 0.50 ±0.07 and H_2O/SO_2 of 174 ± 43.5.

(3) In order to understand the physical and chemical characteristics of the passive and active degassing at Yasur, we consider the gas compositions in the context of a volatile degassing model derived from melt inclusion studies (Metrich et al., 2011). We envisage Yasur's shallow conduit consisting of a crystal-rich region with a thickness of at least 0.6 km, and up to 2 km from the surface. Magmatic gas bubbles (with a slight CO_2-enrichment over gases closer to the surface, and poor in HCl) accumulate at the base of the crystal-rich plug, before generating a local overpressure that is sufficient to overcome the yield strength of the overlying crystal plug.

Acknowledgements

We thank the Vanuatu Meteorology and Geohazards department for their collaboration and support for during access and permission performing a field campaign at Yasur Volcano. Furthermore, we gratefully acknowledge the loan of equipment to carry out this research from the Natural Environment Research Council Field Spectroscopy Facility and their help in during the fieldwork when any questions arose. We also thank Kelson and Rodga from Jungle Oasis for their help during our stay on Tanna island. This work was supported by the Natural

Environment Research Council (grant number NE/L002507/1), by the postgraduate travel funds received from Fitzwilliam College, by the Elspeth Matthews grant given by the Royal Geological Society, by the Mary Euphrasia Mosley, Sir Bartle Frere and Worts travel fund report given by the University of Cambridge and by the Exzellenzstipendium received by WKO. A.A. acknowledges funding support from the Alfred P. Sloan Foundation via the Deep Carbon Observatory (UniPa-CiW subcontract 10881-1262) and from MIUR (under grant n. PRIN2017-2017LMNLAW). T.D.P. acknowledges the support of the Royal Society (RG170226). TI is a Commonwealth Rutherford Fellow, funded by the UK government. We thank two anonymous reviewers, whose helpful comments improved the manuscript enormously.

References

Aiuppa, A., Guidice, G., Gurrieri, S., Liuzzo, M., Burton, M., Caltabiano, T., McGonigle, A,J.S., Salerno, G., Shinohara, H., Valenza, M., 2008. Total volatile flux from Mount Etna. J. Geophys. Res. Lett. 35, L24302

Aiuppa, A., Bertagnini, A., Metrich, N., Moretti, R., Di Muro, A., Liuzzo, M., Tamburello, G., 2010. A model of degassing for Stromboli volcano. Earth Planet. Sci. Lett. 294, 195-204.

Aiuppa, A., de Moor, J. M., Arellano, S.,Coppola, D., Francofonte, V., Galle, B., Moretti, R., 2018. Tracking formation of a lava lake from ground and space: Masaya volcano (Nicaragua), 2014–2017. Geochem. Geophys. Geosyst.19, 496–515.

Aiuppa, A., Fischer, T.P., Plank, T., Bani, P., 2019. CO_2 flux emissions from the Earth's most actively degassing volcanoes, 2005-2015. Sci. Rep. 9(5442).

Allard, P., Carbonelle, J., Metrich, N., Loyer, H., Zettwoog, P., 1994. Sulphur output and magma degassing budget of Stromboli volcano. Nature 368, 326-330.

Allard, P., Burton, M.R., Mure, F., 2005. Spectroscopic evidence for a lava fountain driven by previously accumulated magmatic gas, Nature 433, 407–410.

Allard, P., A CO_2-rich gas trigger of explosive paroxysms at Stromboli basaltic volcano, Italy. 2010. J. Volcanol. Geotherm. Res. 189, 363-374.

Andres, R.J., Kasgnoc, A.D., 1998. A time-averaged inventory of subaerial volcanic sulfur emissions. , J. Geophys. Res. 103, 25251-25261.

Bani, P., Lardy, M., 2007. Sulphur dioxide emission rates from Yasur volcano, Vanuatu archipelago. Geophys. Res. Lett. 34.

667 Bani, P., Harris, A. J.L., Shinohara, H., Donnadieu, F., 2013. Magma dynamics feeding Yasur's
668 explosive activity observed using thermal infrared remote sensing. Geophys. Res. Lett. 40,
669 3830-3835.
670
671 Barth, A., Edmonds, E., Woods. A.W., 2019. Valve-like dynamics of gas flow through a
672 packed crystal mush and cyclic strombolian explosions. Sci Rep. 9(1), 821.
673
674 Batchelor, G.K., 1967. An Introduction to Fluid Dynamics. Cambridge University Press, 615
675 pp
676
677 Battaglia, J., Metaxian, J.P., Garaebiti, E., 2016. Families of similar events and modes of
678 oscillation of the conduit at Yasur volcano (Vanuatu). J. Volcanol. Geotherm. Res. 322, 196-
679 211.
680
681 Battaglia, J., Métaxian,J.P., Garaebiti ,E., 2016. Short term precursors of Strombolian
682 explosions at Yasur volcano (Vanuatu), Geophys. Res. Lett. 43
683
684 Blackburn E.A., Wilson, L., Sparks, R.S.J., 1976. Mechanism and dynamics of Strombolian
685 activity. J.Geol. Soc. Lond. 132, 429-440.
686
687 Beckett, F.M., Burton, M., Mader, H.M., Phillips, J.C., Polacci, M., Rust, A.C., Witham, F.,
688 2014. Conduit convection driving persistent degassing at basaltic volcanoes. J. Volcanol.
689 Geotherm. Res. 238, 19-35.
690
691 Belien, I.B., Cashmann, K.V., Rempel, A.W., 2010. Gas accumulation in particle-rich
692 suspensions and implications in crystal-rich magma. Earth Planet. Sci. Lett. 297, 133-140.
693
694 Bell, R.J., 1972. Introductory Fourier transform spectroscopy. Academic Press, Inc., New
695 York.

696 Burton, M. R., Oppenheimer,C., Horrock,L.A., Francis, P.W., 2000. Remote sensing of CO2
697 and H2O emission rates from Masaya volcano, Nicaragua. Geology 28, 915 – 918.

698 Burton, M., Allard, P., Mure, F., La Spina, A., 2007a. Magmatic gas composition reveals the
699 source depth of slug-driven Strombolian explosive activity. Science 317, 227-230.
700
701 Burton, M.R., Mader, H.M., Polacci, M., 2007b. The role of gas percolation on quiescent
702 degassing of persistently active basaltic volcanoes Earth Planet. Sci. Lett. 262, 46-60.
703
704 Burton, M.R., Sawyer, G.M., Granieri, D., 2013. Deep Carbon Emissions from Volcanoes.
705 Rev. Mineral. Geochem.75, 323-354.
706
707 Capponi, A., James, M.R., Lane, S.J., 2016. Gas slug ascent in a stratified magma: Implications
708 of flow organisation and instability for Strombolian eruption dynamics. Earth Planet. Sci.435,
709 159-170.
710
711 Carn, S.A., Fioletov, V.E., Mc.Linden, C.A., Li, C., Krotov, N.A., 2017. A decade of global
712 volcanic SO2 emissions measured from space. Sci Rep. 7.
713

714 Carney, J., Macfarlane, A., 1979. Geology of Tanna, Aneityum Futana and Aniwa. New
715 Hebrides Gov. Geol. Surv.Rep. 5-29.

716 Chouet, B., Saccorotti, G., Dawson, P., Martini, M., Scarpa, R., DeLuca, G., Milana, G.,
717 Cattaneo, M., 1999. Broadband measure-ments of the sources of explosions at Stromboli
718 volcano, Italy. Geophys. Res. Lett. 26, 1937–1940.

719 Chouet, B., Dawson, P., Ohminato, T., Martini, M.,Saccorotti, G., Giudicepietro, F., De
720 Luca, G., Milana,G., Scarpa, R., 2003. Source mechanisms of explosions at Stromboli
721 Volcano, Italy, determined from moment-tensor inversions of very-long-period data. J.
722 Geophys. Res. 108.

723 Cimarelli, C., Costa, A., Mueller, S., Mader, H.M., 2011. Rheology of magmas with bimodal
724 crystal size and shape distributions: Insights from analogue experiments. Geochem. Geophys.
725 Geosyst.12, 1525-2027.
726
727 Coltelli, M., Del Carlo, P., Vezzoli, L., 1995, Stratig-raphy of the Holocene Mt. Etna explosive
728 eruptions: Periodico di Mineralogia, 64, 141–143.
729
730 Del Bello, E., Llewellin, E., Taddeucci, J., Scarlato, P., Lane, J. S., 2012. An analytical model
731 for gas overpressure in slug-driven explosions: Insights into Strombolian volcanic eruptions.
732 J.Geophys.Res. 117.
733
734 Duffell, H.J., Oppenheimer, C., Pyle, D.M., Galle, B., McGonigle, A.J.S., Burton, M.R., 2003.
735 Changes in gas composition prior to minor explosive eruption at Masaya volcano, Nicaragua.
736 J. Volcanol. Geotherm. Res. 126, 327-339.
737
738 Del Gaudio, P., Ventura, G., Taddeucci, J., 2013. The effect of particle size on the rheology of
739 liquid-solid mixtures with the application to lava flows: Results from analogue experiments.
740 Geochem. Geophys. Geosyst.14, 2661-2669.
741
742 Francis, P. W., Oppenheimer, C., Stevenson, D., 1993. Endogenous growth of persistently
743 active volcanoes. Nature 366, 554–557.
744
745 Francis, P., and Oppenheimer, C., 2004. Volcanoes, 2nd Edition, Oxford University Press,
746 Oxford, 521 pp.
747
748 Ghiorso, M.S., and Sack, R.O., 1995. Chemical mass transfer in magmatic processes IV. A
749 revised and internally consistent thermodynamic model for the interpolation and extrapolation
750 of liquid-solid equilibria in magmatic systems at elevated temperatures and pressures.
751 Contributions Mineral. Petrol. 1999, 197-212.
752
753 Girona, T., Costa, F., Schubert, G., 2015. Degassing during quiescence as a trigger of magma
754 ascent and volcanic eruptions. Sci.Rep. 5, 18212.
755
756 Gaudin, D., Taddeucci, J., Scarlato, P., Moroni, M., Freda, C., Gaeta, M., Palladino, D.M.,
757 2014. Pyroclastic tracking velocimetry illuminates bomb ejection and explosion dynamics at
758 Stromboli (Italy) and Yasur (Vanuatu) volcanoes. J.Geophys. Res. 119, 5384-5397.
759

Gaudin, D., Taddeucci, J., Houghton, B.F., Orr, T.R., Andronico, D., Del Bello, E., Kueppes, U., Ricci, T., Scarlato, P., 2016. 3-D high speed imaging of volcanic bomb trajectory in basaltic explosive eruptions. Geochem. Geophys. Geosyst.17, 4268-4275.

Gaudin, D., Taddeucci, J., Scarlato, P., Del Bello, E., Ricci, T., Orr, T., Houghton, B., Harris, A.J.L., Rao, S., Bucci, A., 2017. Integrating puffing and explosions in a general scheme for Strombolian-style activity. J. Geophys. Res. Solid Earth 122 (3), 1860–1875.

Getson, J.M., Whittington, A.G., 2007. Liquid and magma viscosity of anorthite-forsterite-diopside-quartz systems and implications for the viscosity-temperature paths of cooling magmas. J.Geophys.Res.112.

Griffiths, P.R., 1975. Chemical infrared Fourier transform spectroscopy, Chemical analysis. Wiley, New York.

Gurioli, L., Colo, L., Bollasina, A.J., Harris, A.J.L., Whittington,A., Ripepe, M., 2014. Dynamics of Strombolian explosions: Inferences from field and laboratory studies of erupted bombs from Stromboli volcano, J. Geophys. Res. Solid Earth, 119, 319–345.

Harrocks, L. A., Oppenheimer, C., Burton, M.R., Duffell, H.J., Davies, N.M., Nicholas, A,M., Bell, W., 2001. Open-path Fourier transform infrared spectroscopy of SO_2: An empirical error budget analysis, with implications for volcano monitoring. J.Geophys. Res. 106, 27647-27659.

Harris, A.J.L., Stevenson, D.S., 1997. Magma budgets and a steady-state activity of Vulcano and Stromboli. Geophys. Res. Lett. 24, 1043-1046.

Hort, M., Seyfried, R., Voge, M., 2003. Radar Doppler velocimetry of volcanic eruptions: theoretical considerations and quantitative documentation of changes in eruptive behaviour at Stromboli volcano, Italy. Geophys.J. Int. 154, 515–532**.**

Houghton, B.F., and Gonnermann, H.M., 2008. Basaltic explosive volcanism: Constraints from deposits and models. Chem Erde-Geochem.68, 117-140.

Houghton, B.F., Taddeucci, J., Andronico, D., Gonnermann, H.M., Pistolesi, M., Patrick, M.R., Orr, T.R., Swanson, D.A., Edmonds, M., Gaudin, D., Carey, R.J., Scarlato, P., 2016. Stronger or longer: discriminating between Hawaiian and Strombolian eruption styles. Geology 44, 163–166.

Huppert, H.E., Hallworth, M.A., 2007. Bi-directional flows in constrained systems. J. Fluid Mech. 578, 95–112.

Ilanko, T., Opppenheimer, C., Burgisser, A., Kyle, P., 2015. Transient degassing events at the lava lake at the lava lake of Erebus volcano. GeoResJ, 7, 43-48.

Ilanko, T., Pering, T.D., Wilkes, T.C., Woitischek, J., D'Alea, R., Aiuppa, A., McGonigle, A.J.S., Edmonds, M., Garaebaeti, E., 2020. Ultraviolet camera measurments of passive and explosive sulphur dioxide emissions at Yasur volcano, Vanuatu. http://eartharxic.org/7r2ay.

Ilyinskaya, E., Martin, R.S., Oppenheimer, C., 2012. Aerosol formations in basaltic lava fountaining: Eyjafjallajökull volcano, Iceland. J.Geophys. Res. 117.

James, M.R., Lane, S.J., Wilson, L., Corder, S.B., 2009. Degassing at low magma-viscosity volcanoes: Quantifying the transition between bubble-burst and Strombolian eruption. J. Volcanol. Geotherm. Res., 180, 81-88.

Jaupart, C., Vergniolle, S., 1989. The generation and collapse of a foam layer at the roof of a basaltic magma chamber. J. Fluid Mech. 203, 347-380.

Jaupart, C., Vergniolle, S., 1988. Laboratory models of Hawaiian and Strombolian eruptions. Nature 331, 58-60.

Kantzas, E.T., McGonigle, A.J.S., Tamburello, G., Aiuppa, A., Bryant, R.G., 2010. Protocols for UV camera volcanic SO_2 measurements. Volcanol. Geotherm. Res. 194, 55-60.

Kazahaya, K., Shinohara, H., Saito, G., 1994. Excessive degassing of Izu-Oshima volcano: magma convection in a conduit. Bull. Volcanol. 56, 207-216.

Kern, C., Luebcke, P., Bobrowski, N., Campion, R., Mori, T., Smekesn, J., Stebel, K., Tamburello, G., Burton, M., Platt, U., Prata, F., 2015. Intercomparison of SO_2 camera system for imaging volcanic gas plumes. Volcanol. Geotherm. Res. 300, 22-36.

Kremers, S., Lavallée, Y., Hanson, J., Hess, K. U., Chevrel, M. O., Wassermann, J., Dingwell, D. B., 2012. Shallow magma-mingling-driven Strombolian eruptions at Mt. Yasur volcano, Vanuatu Geophys. Res. Lett. 39(21).

Koyaguchi, T., 1985, Magma mixing in a conduit. J.Volcanol. Geotherm. Res. 25, 365-369.

Koyaguchi, T., 1987, Magma mixing in a squeezed conduit. Earth Planet. Sci. Let. 84, 339-744.

Liu, E.J., Wood, K., Mason, E., Edmonds, M., Aiuppa, A., Guidice, G., Bitetto, M., Francofonte, V., Burrow, S., Richardson, T., Watson, M., Pering, T.D., Wilkes, T.C., McGonigle, A.J.S., Velasquez, G., Melgarejo, C., Bucarey, C., 2019. Dynamics of Outgassing and Plume Transport Revealed by Proximal Unmanned Aerial Systems (UAS) Measurements at Volcan Villarrica, Chile. Geochem. Geophys. Geosyst,. 20,730–750.

Louat, R., Hamburger, M., Monizier, M., 1988. Shallow and intermediate-depth seismicity in the New Hebrides arc: Contrains on the subduction process. In: Greene,H.G., Wong, F.L (Eds), Geology and Offshore Resources of Pacific Island Arcs- Vanuatu Region. Circum-Pac. Counc. For energy and Miner. Res., Houston, Tex., earth. Sci. Ser. 8, 329-356.

Martin. R.S., Sawyer, G.M., Spampinato, L., Salerno, G.G., Ramirez, C., Ilyinskaya, I., Witt, M.L.I., Mather, T.A., Watson, I.M., Phillips, J.C., Oppenheimer, C., 2010. A volatile inventory for Masya Volcano, Nicaragua. Geophys. Res. 115, B09215,

Meier, K., Hort, M., Wassermann, J., Garaebiti, E., 2016. Strombolian surface activity regimes at Yasur volcano, Vanuatu, as observed by Doppler radar infrared camera and infrasound. J. Volcanol. Geotherm. Res. 322, 184-195.

Metrich, N., Allard, P., Aiuppa, A., Bani, P., Bertagnini, A., Shinohara, H., Parello,F., Di Muro, A., Garaebiti, E., Belhadj,O., Massare, D., 2011. Magma and volatile supply to post-collapse volcanism and block resurgence in Siwi Caldera (Tanna island, Vanuatu Arc). J.Petrol. 52, 1077-1105.

Mori, T., Burton, M., 2006. The SO_2 camera: A simple, fast and cheap method for ground based imaging of SO_2 in volcanic plumes. Geophys. Res. Lett.33.

Mori, T., Burton, M., 2009. Quantification of the gas mass emitted during single explosions on Stromboli with the SO_2 camera. J. Volcanol. Geotherm. Res. 188, 395-400.

Neuberg, J., Luckett, R., Ripepe, M., Braun, T., 1994. Highlights from a seismic broadband array on Stromboli volcano. Geophys.Res. Lett. 21, 749–752.

Ntepe, R., Dorel, J., 1990. Observation of seismic volcanic signals at Stromboli Volcano (Italy). J. Volcanol. Geotherm. Res. 43, 235-251.

Oppenheimer, C., 1996. On the role of hydrothermal systems in the transfer of volcanic sulfur to the atmosphere. Geo- phys. Res. Lett. 23, 2057-2060.

Oppenheimer, C., *Volcanic degassing*, In: *The Crust*, Vol. 3, *Treatise on Geochemistry*. 2003. ed. by R.L. Rudnick, H.D. Holland, K.K. Turekian. Elsevier-Pergamon, Oxford, 123–166 .

Oppenheimer, C., Bani, P., Calkins, J.A., Burton, M.R., Sawyer, G.M., 2006. Rapid FTIR sensing of volcanic gases released by Strombolian explosions at Yasur volcano. Applied Physics B, Volume 85, Issue 2-3, 453-460.

Oppenheimer, J., Rust. A.C., Cashman, K.V., Sandnes, B., 2015. Gas migration regimes and outgassing in particle-rich suspensions. Front. Phys. 3:60.

Oppenheimer, J., Capponi, A., Cashman, K.V., Lane, S.J., Rust, A.C., James, M.R., 2020. Analogues experiments on the rise of large bubbles through a solids-rich suspension: A “weak plug” model for Strombolian eruptions. Earth Planet. Sci. Lett 531, 115931.

Patrick, M.R., Harris, A., Ripepe, M., Dehn, J., Rothery, D.A., Calvari, S., 2007. Strombolian explosive styles and source conditions: Insights from thermal (FLIR) video. Bull. Volcanol. 69 (7), 769–784.

Parfitt, E.A., Wilson, L., 1995. Explosive volcanic eruptions:IX. The transition between Hawaiian-style lava fountaining and Strombolian explosive activity. Geophys. J. Int. 121,226–232.

Parfitt, E. A., 2004. A discussion of the mechanisms of explosive basaltic eruptions. J. Volcanol. Geotherm. Res. 134, 77-107.

Parfitt, E.A., Wilson, L., 2008. Fundamentals of physical volcanology. Blackwell Publishing Ltd. 230pp.

Parmigiani, A., Huber, C., Bachmann, O., 2014. Mush microphysics and the reactivation of crystal-rich magma reservoirs. J.Geophys. Res. Solid Earth 119, 6308-6322.

Parmigiani, A., Faroughi S., Huber, C., Bachmann, O., Su, Y., 2016. Bubble accumulation and its role in the evolution of the magma reservoirs in the upper crust. Nature 532, 492-495.

Parmigiani, A., Degruyter, W., Leclaire, S., Huber, C., Bachmann, O., 2017. The mechanics of shallow magma reservioir outgassing. Geochem. Geophys. Geosyst. 18, 2887-2905.

Patrick, M.R., Harris, A.J.L., Ripepe, M., Dehn, J., Rothery, D., Calvari, S., 2007. Strombolian explosive styles and source conditions: insights from thermal (FLIR) video. Bull. Volcanol. 69, 769–784.

Pering, T.D., Tamburello, G., McGonigle, A.J.S., Aiuppa, A., James, M.R., Lane, S.J., Sciotto, M., Cannata, A., Patane, D., 2015. Dynamics of mild strombolian eruptions on Mt. Etna. J. Volcanol. Geotherm. Res. 300, 103-111.

Pering, T.D., McGonigle, A.J.S., 2018. Combining Spherical-Cap and Taylor Bubble Fluid Dynamics with Plume Measurements to Characterize Basaltic Degassing. Geoscience 8 (2), 42.

Pioli, L., Bonadonna,C., Azzopardi, B.J., Phillips,J.C., Ripepe, M., 2012. Experimental constraints on the outgassing dynamics of basaltic magmas, J. Geophys. Res. 117, B03204,

Pistone, M., Whittington, A. G., Andrews, B. J., Cottrell, E. 2017. Crystal-rich lava dome extrusion during vesiculation: an experimental study. J. Volcanol.Geotherm. Res. 347, 1–14.

Ripepe, M., Marchetti, E., 2002. Array tracking of infrasonic sources at Stromboli volcano. Geophys. Res. Lett. 29.

Ripepe, M., Rossi, M., Saccorotti, G., 1993. Image processing of explosive activity at Stromboli, J. Volcanol. Geotherm. Res. 54, 335–351.

Ripepe, M., Marchetti, E., Ulivieri, G., 2007. Infrasonic monitoring at Stromboli volcano during the 2003 effusive eruption: insights on the explosive and degassing processof an open conduit system. J.Geophys. Res. 112, B09207.

Ripepe, M., Harris, A.J.L., 2008. Dynamics of the 5 April 2003 explosive paroxysm observed at Stromboli by a near-vent thermal, seismic and infrasonic array. Geophys. Res. Lett. 35 , L07306.

Rothman, L.S., Gordon, I.E., Barbe, A., Chris Benner, D., Bernath, P.F., Birk, M., Boudon, V., Brown, L.R., Campargue, A., Champion, J.-P., Chance, K., Coudert, L.H., Dana, V., Devi, V.M., Fally, S., Flaud, J.-M., Gamache, R.R., Goldman, A., Jacquemart, D., Kleiner, I., Lacome, N., Lafferty, W.J., Mandin, J.-Y., Massie, S.T., Mikhailenko, S.N., Miller, C.E., Moazzen-Ahmadi, N., Naumenko, O.V., Nikitin, A.V., Orphal, J., Perevalov, V.I., Perrin, A., Predoi-Cross, A., Rinsland, C.P., Rotger, M., Simeckova, M., Smith, M.A.H., Sung, K., Tashkun, S.A., Tennyson, J., Toth, R.A., Vandaele, A.C., Vander Auwera, 2009. The HITRAN 2008 molecular spectroscopic database. J. Quant. Spectrosc. Radiat. Transfer 110:533–572.

Rosi, M., Pistolesi, M., Bertagnini, A., Landi, P., Pompilio, M., Di Roberto, A., 2013. Stromboli Volcano, Aeolian Islands (Italy): Present Eruptive Activity and Hazards. Geological Society London Memoirs 37(1), 473–490.

Sawyer, G.M., Salerno, G.G., Le Bond, J.S., Martin, R.S., Spampinato, L., Roberts, T.J., Mather, T.A., Witt, M.L.I., Tsanev, V.I., Oppenheimer, C., 2011. Gas and aerosol emissions from Villarrica volcano, Chile. J. Volcanol. Geotherm. Res. 203, 62-75.

Shinohara, H., 2005. A new technique to estimate volcanic gas composition: plume measurements with a portable multi-sensor system. J. Volcanol. Geotherm. Res. 143(4), 319–333.

Slezin, Y.B., 2003. The mechanism of volcanic eruptions (a steady state approach). J. Volcanol. Geotherm. Res. 122, 7–50.

Sparks, R.S.J., 1978. The dynamics of bubble formation and growth in magmas: A review and analysis. J. Volcanol. Geotherm. Res. 3, 1-37.

Spina, L., Taddeucci, J., Cannata, A., Gresta, S., Lodato, L., Privitera, E., Scarlato, P., Gaeta, M., Gaudin, D., Palladino, D.M., 2016. Explosive volcanic activity at Mt. Yasur: A characterization of the acoustic events (9-12th July 2011). J. Volcanol. Geotherm. Res. 322, 174-183. Spina, L., Morgavi, D., Costa, A., Scheu, B., Dingwell, D. B., & Perugini, D., 2019b. Gas mobility in rheologically-layered volcanic conduits: The role of decompression rate and crystal content on the ascent dynamics of magmas. Earth Planet. Sci. 524, 115732.

Stevenson, D.S., Blake, S., 1998. Modelling the dynamics and thermodynamics of volcanic degassing. Bull. Volcanol. 60, 307–317.

Seyfried, R., Hort, M., 1999. Continuous monitoring of volcanic eruption dynamics: a review of various techniques and new results from a frequency-modulated radar Dopplersystem. Bull. Volcanol. 60, 627–639.

Symonds, R.B., Rose, W.I., Bluth, G.J.S., and Gerlach,T.M., 1994. Volcanic gas studies: Methods, results, and applications ,in Carroll, M.R., et al.,eds., Volatiles in magmas: Reviews in Mineralogy, v. 30, p. 1–66.

Taddeucci. J., Scarlato, P., Capponi, A., Del Bello, E., Cimarelli, C., Palladino, D.M., Keuppers, U., 2012a. High-speed imaging of Strombolian explosions: The ejection velocity of pyroclasts. Geophys.Res.Lett. 39 (L02) 301.

Taddeucci, J., Alatoore-Ibarguengorita, M.A., Moroni, M., Tornetta, L., Capponi, A., Scarlatto, P., Dingwell, D.B., De Rita, D., 2012 b. Physicalparameterization of Strombolian eruptions via experimentally-validated modeling of high-speed observations. Geophys. Res. Lett. 39, L16306.

Tamburello, G., Aiuppa, A., Kantzas, E.P., McGonogle, A.J,S., Ripepe, M., 2012. Passive vs. active degassing modes at an open-vent volcano (Stromboli, Italy). Earth Planet. Sci. Lett. 249-360, 106-116.

Tamburello, G., 2015. Ratiocalc: Software for processing data from multicomponent volcanic gas analyzers. Comput.Geosci.82, 63-67.

Taylor, G.A., 1956. Review of volcanic activity in the Territory of Papua-New Guinea-the Solomon and New-Hebrides Islands,1951-1953. Bull.Volcanol., II/XVII, 33-37.

Urbanski, N., Voege, M., Seyfried, R., Ruepke, L., Petersen, T., Hanebuth,T. Hort, M., 2002. 15 days of continuous activity survey at Stromboli volcano/Italy in late September 2000: Doppler radar, seismicity, infrared, soil humidity, and mapping of the crater region. Int. J. Earth Sci. 91, 712–721.

Vergniolle, S., Brandeis, G., Marechal. 1996. Strombolian explosions 2: Eruption dynamics determined from acoustic measurements. J. Geophys. Res. 101 (B9), 20449-20466.Vergniolle, S., Ripepe, M., 2008, From Strombolian explosions to fire fountains at Etna Volcano (Italy): What do we learn by acoustic measurement?, in Fluid Motions in Volcanic Conduits: A Source of Seismic and Acoustic Signals, edited by S. J. Lane and J. S. Gilbert, Geol. Soc. Spec.Publ. 307, 103–124.

Vergniolle, S., Metrich, N., 2016. A bird's eye view of "Understanding volcanoes in the Vanuatu arc". J. Volcanol. Geotherm. Res. 322, 1-5.

Walker, G. P. L., Self, S., and Wilson, L., 1984, Tarawera, 1886, New Zealand-A basaltic plinian fissure eruption. J. Volcanol. Geotherm. Res. 21, 61–78.

Williams, S. N., 1983, Plinian airfall deposits of basaltic composition: Geology, 11, 211–214.

Wilkes, C.T., Pering, T.D., McGonigel, A,J.S., Tamburello, G., Willmott, J.R., 2017. A Low-Cost Smartphone Sensor-Based UV Camera for Volcanic SO_2 Emission Measurements. Remote Sens. 2017, 9(1), 27.

Wilkes, T.C., McGonigle, A.J.S., Pering, T.D., Taggart, A.J., White, B.S., Bryant, R.G., Willmott, J.R., 2016. Ultraviolet Imaging with Low Cost Smartphone Sensors: Development and Application of a Raspberry Pi-Based UV Camera. Sensors 16, 1649.

Wilson, L., Head, J.W., 1981. Ascent and eruption of basaltic mag-ma on the Earth and Moon. J. Geophys. Res. 86, 2971–3001.

Wilson, L., Head, J.W., 1983. A comparison of volcanic eruption processes on Earth, Moon, Mars, Io and Venus. Nature 302,663–669.

Woods, A.W., and Cardoso, S.S.S., 1997. Triggering basaltic volcanic eruptions by bubble-melt separation. Nature 385, 518-20.